Implementation and Application of the Frozen Density Embedding Theory with the Algebraic Diagrammatic Construction Scheme for the Polarization Propagator up to Third Order

Prager, Stefan; Zech, Alexander; Wesolowski, Tomasz Adam; Dreuw, Andreas

How to cite

PRAGER, Stefan et al. Implementation and Application of the Frozen Density Embedding Theory with the Algebraic Diagrammatic Construction Scheme for the Polarization Propagator up to Third Order. In: Journal of Chemical Theory and Computation, 2017, vol. 13, n° 10, p. 4711–4725. doi: 10.1021/acs.jctc.7b00461

This publication URL: https://archive-ouverte.unige.ch/unige:98053
Publication DOI: 10.1021/acs.jctc.7b00461

Implementation and application of the frozen density embedding theory with the algebraic diagrammatic construction scheme for the polarization propagator up to third order

Stefan Prager,*,† Alexander Zech,‡ Tomasz Wesolowski,‡ and Andreas Dreuw*,†

Interdisciplinary Center for Scientific Computing, Ruprecht-Karls University, Im Neuenheimer Feld 205A, 69120 Heidelberg, Germany, and Dèpartement de Chimie Physique, Université de Genève, 30 quai Ernest-Ansermet, 1211 Genève, Switzerland

E-mail: stefan.prager@iwr.uni-heidelberg.de; dreuw@uni-heidelberg.de

Abstract

Implementation, benchmarking and representative applications of the new FDE-ADC(3) method for describing environmental effects on excited states as a combination of frozen density embedding (FDE) and the algebraic-diagrammatic construction scheme for the polarization propagator of third order (ADC(3)). Results of FDE-ADC(3) calculations are evaluated with respect to supersystem calculations on test systems with varying molecule - environment interaction strengths from dispersion up to multiple hydrogen bonds. The overall deviation compared to the supersystem calculations is as small as 0.029 eV for excitation energies, which is even smaller than the

*To whom correspondence should be addressed
†Heidelberg University
‡Geneva University

intrinsic error of ADC(3). The dependence of the accuracy on the choice of method and functional for the calculation of the environment and the non-electrostatic part of the system-environment interaction is evaluated. In three representative examples, the FDE-ADC method is applied to investigate larger systems and to analyze excited state properties using visualization of embedded densities and orbitals.

Table of Contents Graphic

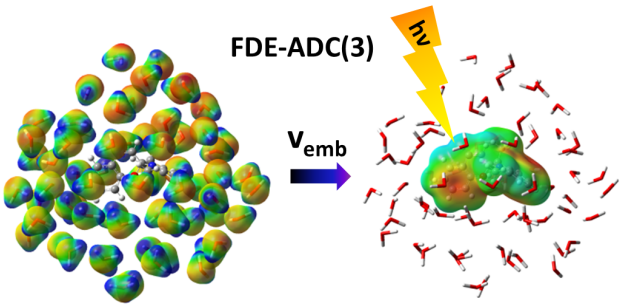

Keywords: Density Embedding, Algebraic-Diagrammatic Construction Scheme, Excited States, Environment, Polarization Propagator

1 Introduction

Most easily, quantum chemical calculations are carried out in the gas phase, but most experimental results are obtained in solution or solid phase. Therefore, including the effects of the environment on chemical and physical properties of the investigated molecule in calculations becomes more and more important. Especially electronically excited states are prone to influences of an environment. Excitation energies can be and usually are shifted, an effect known as solvatochromism.[1] A full supermolecular quantum chemical treatment of a molecule and its environment, however can easily exceed the limits of feasible calculations due to the high scaling factors of state of the art *ab initio* methods. Hence, further approximations for including the effects of environments are required to be made.

Mainly two different approaches for including the environment in an approximative way have been established: the implicit and explicit solvent models. In the former, the environment is usually described as a homogeneously polarizable medium, like in polarizible continuum models (PCM),[2] while the latter one describes the molecules of an environment explicitely. This allows for the modeling of specific solute-solvent interactions, for instance hydrogen bonds, which cannot correctly be described using implicit models.[3,4] An example for explicit solvent interaction is the typical QM/MM approach.[5]

A more recent development in the framework of explicit environment models is represented by density embedding methods.[6–9] In Frozen Density Embedding Theory (FDET)[6,10] in particular, the system is divided into two parts: the embedded system (A) and the environment (B). A is then seen as embedded into the electronic density of system B, which is kept unchanged (*frozen*). The embedded system A can be treated on DFT level of theory,[11–13] but also, as shown in more recent developments, using wavefunction based methods.[7,10,14–17] The density of the environment is usually obtained from lower level quantum chemical calculations,[10] theories for ensembles,[18] or even from experiment.[9] An embedding potential is then created using the environment density as well as the density of the embedded system ($\rho_A(\vec{r})$). In standard form of FDET, herein referred to as *conventional FDET*, an iterative scheme is

needed to create an embedding potential which is self-consistent with the wavefunction or density of system A.[16,17,19,20]

The FDET variant used in our approach depends on a reference density of A ($(\rho_A^{ref}(\vec{r})$) and will herein referred to as *linearized FDET*.[21,22] This facilitates the use of the same embedding potential for all electronically excited states, as it circumvents its state dependence and maintains orthogonality between the states. It can be used in combination with TD-DFT and wavefunction-based excited state methods, the latter of which lead to more systematic and reliable calculations owing to the known limitations of TD-DFT.[23–25]

In this context, the algebraic diagrammatic construction scheme (ADC) for the polarization propagator in third order is an established and accurate method to calculate electronically excited states.[26,27] Since it is based on perturbation theory and on a non-iterative ground state method, the inclusion of external one-particle potentials via the Fock operator is quite straight-forward. The ADC(3) method is Hermitian, size-consistent and systematically improvable.[28]

In previous work, we have presented the first combination of FDET and ADC(2).[29] In this article, we briefly review the theory of ADC and FDET in section 2. In section 3 we present the implementation of FDE-ADC in a quantum chemical software package. In section 4 our results are presented. While in subsection 4.1 the best choice of xc-functional for the calculation of the embedding potential is investigated, subsection 4.2 is denoted to benchmarking of the new FDE-ADC(3) method. In section 5 representative applications of FDE-ADC methods are shown. The paper concludes with a summary of the main results of our work in section 6.

2 Theoretical Methodology

2.1 Algebraic Diagrammatic Construction Scheme for the Polarization Propagator

The algebraic diagrammatic construction scheme for the polarization propagator (ADC) is a size-extensive and Hermitian method for calculation of vertically excited correlated electronic states. It is based on the Møller-Plesset partitioning of the Hamilton operator and can therefore be seen as "perturbation theory for excited states". A full derivation of ADC is given in the literature.[30–34] As shown previously,[28] ADC can be derived using the intermediate state (IS) formalism. In this representation the ADC matrix is given as the Hamilton-Operator shifted by the ground state energy E_0

$$M_{IJ} = \langle \tilde{\Psi}_I | \hat{H} - E_0 | \tilde{\Psi}_J \rangle, \tag{1}$$

which leads to a Hermitian eigenvalue problem

$$\mathbf{MX} = \mathbf{X\Omega}, \qquad \mathbf{X}^\dagger\mathbf{X} = \mathbf{1}. \tag{2}$$

with $\mathbf{X}$ as the matrix of eigenvectors, corresponding to the excited states and $\mathbf{\Omega}$ as the matrix of eigenvalues, corresponding to the excitation energies. In general, the order of perturbation theory used for the construction of the ISR determines the order of the ADC scheme. Using 2nd order perturbation theory (MP(2)) in the IS formalism results in the 2nd order ADC equations (ADC(2)), using 3rd order perturbation theory (MP(3)) yields 3rd order ADC equations (ADC(3)).[27,28,30,33,34]

2.2 Frozen Density Embedding Theory (FDET)

Frozen Density Embedding Theory (FDET) has been previously derived in literature,[10,22] however, for completeness, a brief introduction is given in this section. In FDET, the supersystem is divided into the embedded system (A) and the environment (B). The density of the environment, once obtained, is kept frozen through the whole calculation. A so-called embedding potential v_{emb} is created from the densities of both subsystems. This potential is used as an external potential for the embedded system A, i.e. A is embedded in the density of B. Since FDET exhibits similarities to QM/MM approaches, it shares its limitations. One can not easily break covalent bonds when dividing a supersystem into the two fragments. Also, electronic processes including both fragments, like charge-transfer excitation form fragment A to B are difficult to be modeled. Hence, standard FDET is only applicable for systems amenable for QM/MM type of embedding methods.

In this work, A is treated using ADC(3) instead of DFT while the density of B can be computed using either wavefunction- or density-based methods. Thus, the total energy of the supersystem is given as

$$\begin{aligned} E_{AB}^{EWF}[\Psi_A, \rho_B] = \langle \Psi_A | \hat{H}_A | \Psi_A \rangle + V_B^{nuc}[\rho_A] \\ + J_{int}[\rho_A, \rho_B] + E_{xc,T}^{nad}[\rho_A, \rho_B] \\ + E_{v_B}^{HK}[\rho_B] + V_A^{nuc}[\rho_B], \end{aligned} \tag{3}$$

with

$$J_{int}[\rho_A, \rho_B] = \int\int \frac{\rho_A(\vec{r})\rho_B(\vec{r}')}{\left|\vec{r} - \vec{r}'\right|} \mathrm{d}\vec{r}\mathrm{d}\vec{r}' \tag{4}$$

$$V_A^{nuc}[\rho_B] = \int \rho_B(\vec{r}) v_A(\vec{r}) \mathrm{d}\vec{r} \tag{5}$$

$$V_B^{nuc}[\rho_A] = \int \rho_A(\vec{r}) v_B(\vec{r}) \mathrm{d}\vec{r} \tag{6}$$

$$\begin{aligned} E_{xc,T}^{nad}[\rho_A, \rho_B] &= E_{xc}^{nad}[\rho_A, \rho_B] + T_s^{nad}[\rho_A, \rho_B] \\ &\quad + \Delta F^{MD}[\rho_A]. \end{aligned} \tag{7}$$

These terms describe the interaction between the embedded species A and the environment B. $J_{int}[\rho_A, \rho_B]$, $V_A^{nuc}[\rho_B]$ and $V_B^{nuc}[\rho_A]$ correspond to coulombic electron-electron repulsion, attraction between electron density of B with nuclei of A and attraction between electron density of A with nuclei of B, respectively. $E_{xc,T}^{nad}[\rho_A, \rho_B]$ describes a non-additive energy bifunctional and comprises terms for exchange-, correlation- and kinetic density functionals. Typically, the ρ_A-dependent functional $\Delta F^{MD}[\rho_A]$ is neglected in practice since its contributions are usually small.[35] The non-additive energy bifunctional is defined as:

$$E^{nad}[\rho_A, \rho_B] = E[\rho_A + \rho_B] - \left(E[\rho_A] + E[\rho_B]\right). \tag{8}$$

Building the functional derivative of the total energy expression (Eq. 3) with respect to the electron density of A (ρ_A) one obtains the embedding potential v_{emb} which reads:

$$\begin{aligned} &v_{emb}[\rho_A, \rho_B, v_B](\vec{r}) \\ &\quad = v_B(\vec{r}) + \int \frac{\rho_B(\vec{r}')}{\left|\vec{r} - \vec{r}'\right|} \mathrm{d}\vec{r}' + \frac{\delta E_{xc,T}^{nad}[\rho_A, \rho_B]}{\delta \rho_A}. \end{aligned} \tag{9}$$

Since the embedding potential, which is used to compute the electron density of system A, depends itself on the density of system A, the resulting equation is non-linear and has to

be solved iteratively. In the further approximated version of FDET, denoted as linearized FDET, the electron density of A (ρ_A) in the embedding potential is replaced by the constant ground state reference density ρ_A^{ref}. Thus the non-additive energy functional $E_{xc,T}^{nad}[\rho_A, \rho_B]$ is replaced by the approximate energy functional depending on ρ_A^{ref} instead of ρ_A[22]

$$E_{xc,T}^{nad}[\rho_A^{ref}, \rho_B] = E_{xc}^{nad}[\rho_A^{ref}, \rho_B] + E_T^{nad}[\rho_A^{ref}, \rho_B]. \tag{10}$$

The approximation is constructed as a Taylor-expansion of the non-additive energy functional around the reference density $\rho_A^{ref}(\vec{r})$ with the series being truncated after the linear term:[22]

$$\begin{aligned} &E_{xc,T}^{nad}[\rho_A, \rho_B] \approx E_{xc,T}^{nad}[\rho_A^{ref}, \rho_B] \\ &+ \int \left(\rho_A(\vec{r}) - \rho_A^{ref}(\vec{r})\right) \frac{\delta E_{xc,T}^{nad}[\rho_A^{ref}, \rho_B]}{\delta \rho_A^{ref}(\vec{r})} \mathrm{d}\vec{r} \\ &= E_{xc,T}^{nad}[\rho_A^{ref}, \rho_B] + \Delta^{lin}[\rho_A, \rho_A^{ref}, \rho_B]. \end{aligned} \tag{11}$$

Then, the total energy expression in linearized FDET is now linear in ρ_A and reads:

$$\begin{aligned} E_{AB}^{LinFDET}[\Psi_A, \rho_B, \rho_A^{ref}] = &\langle \Psi_A | \hat{H}_A | \Psi_A \rangle \\ &+ \int \rho_A(\vec{r}) v_B(\vec{r}) \mathrm{d}\vec{r} \\ &+ \int \rho_B(\vec{r}) v_A(\vec{r}) \mathrm{d}\vec{r} \\ &+ \int\int \frac{\rho_A(\vec{r}) \rho_B(\vec{r}')}{\left|\vec{r} - \vec{r}'\right|} \mathrm{d}\vec{r} \mathrm{d}\vec{r}' \\ &+ E_{xc}^{nad}[\rho_A^{ref}, \rho_B] + T_s^{nad}[\rho_A^{ref}, \rho_B] \\ &+ E_{v_B}^{HK}[\rho_B] \\ &+ \Delta^{lin}[\rho_A, \rho_A^{ref}, \rho_B]. \end{aligned} \tag{12}$$

The corresponding embedding potential is independent of the electronic state of the embed-

ded system A and given as:

$$\begin{aligned} &v_{emb}[\rho_A^{ref}, \rho_B, v_B](\vec{r}) \\ &= v_B(\vec{r}) + \int \frac{\rho_B(\vec{r}')}{\left|\vec{r} - \vec{r}'\right|} \mathrm{d}\vec{r}' + \frac{\delta E_{xc,T}^{nad}[\rho_A^{ref}, \rho_B]}{\delta \rho_A^{ref}}. \end{aligned} \tag{13}$$

This embedding potential will from here on be denoted as $v_{emb}^{lin}(\vec{r})$. It is added to the ground state Hamiltonian resulting in the following Schrödinger-like equation:

$$\left(\hat{H}_A + \hat{v}_{emb}^{lin}\right) \Psi_A = \epsilon \Psi_A \tag{14}$$

In the evaluation of the expectation value of the Hamiltonian, also the expectation value of the embedding potential is calculated, which includes all electrostatic and part of the non-electrostatic terms.

$$\begin{aligned} \langle \Psi_A | \hat{v}_{emb}^{lin} | \Psi_A \rangle = V_B^{nuc}[\rho_A] + J_{int}[\rho_A, \rho_B] \\ + \int \rho_A(\vec{r}) \frac{\delta E_{xc,T}^{nad}[\rho_A^{ref}, \rho_B]}{\delta \rho_A^{ref}(\vec{r})} \mathrm{d}\vec{r} \end{aligned} \tag{15}$$

Thus, for the evaluation of the total energy expression, Eq. 12 can be rewritten as:

$$\begin{aligned} E_{AB}^{LinFDET}[\Psi_A, \rho_B, \rho_A^{ref}] = \langle \Psi_A | \hat{H}_A + \hat{v}_{emb}^{lin}(\vec{r}) | \Psi_A \rangle \\ + \int \rho_B(\vec{r}) v_A(\vec{r}) \mathrm{d}\vec{r} \\ + \Delta F^{MD}[\rho_A^{ref}] + E_{v_B}^{HK}[\rho_B] \\ + E_{xc,T}^{nad}[\rho_A^{ref}, \rho_B] \\ - \int \rho_A^{ref}(\vec{r}) \frac{\delta E_{xc,T}^{nad}[\rho_A^{ref}, \rho_B]}{\delta \rho_A^{ref}(\vec{r})} \mathrm{d}\vec{r} \end{aligned} \tag{16}$$

Hence, after evaluation of the Hamiltonian including the embedding potential, only constant, state-independent terms have to be added. Thus, the excitation energy, which is defined as

the energy difference between different states, simplifies to:

$$\Delta E_{IJ} = \langle \Psi_A^J | \hat{H}_A + \hat{v}_{emb}^{lin} | \Psi_A^J \rangle - \langle \Psi_A^I | \hat{H}_A + \hat{v}_{emb}^{lin} | \Psi_A^I \rangle. \tag{17}$$

because all other terms cancel exactly.

3 Implementation and Computational Methodology

Continuing our previous work,[29] the FDE-ADC algorithm has been implemented as a module called `FDEman` into the quantum chemical program package Q-Chem.[36] In this article, we present for the first time an implementation of FDE-ADC up to third order for both core- and valence excitations, i.e. FDE-ADC(3) and FDE-CVS-ADC(3).

The procedure of an FDE-ADC calculation comprises four steps: *a)* generation of ρ_A, *b)* generation of ρ_B, *c)* calculation of v_{emb}^{lin} and finally *d)* applying v_{emb}^{lin} in an FDE-ADC calculation. In the first step, fragment A is initialized and a density matrix in the basis of atomic orbitals at the corresponding level of Møller-Plesset perturbation theory[37,38](MP) is computed employing the `adcman`[26] module in Q-Chem. This density matrix (ρ_A^{ref}) is stored and in the next step the environment fragment B is initialized, and either a Hartree-Fock (HF)[39] or a density-functional-theory (DFT)[11–13] calculation can be performed to obtain the density matrix ρ_B. In a third step, the two density matrices of A and B are used to evaluate the four state-independent parts of the embedding potential, which are the nuclear attraction potential, the coulombic repulsion potential and the exchange-correlation and kinetic energy non-additive bifunctional potentials. (See Eq. 13) The expectation value as well as the derivative of the non-additive functionals are calculated using integration on a standard quadrature grid SG-1.[40] In the last step, an FDE-ADC calculation is performed using the adcman module. For this purpose, system A is initialized again and the previously generated embedding potential is subsequently added to the Fock-Matrix **F** in the SCF procedure of

the underlying HF calculation.

$$\tilde{\mathbf{F}} = \mathbf{F} + v_{emb}^{lin}. \tag{18}$$

Since the influence of the environment is included in the modified orbitals and orbital energies, no changes have to be made to the ADC equations. Thereby it is immediately available for all variants of ADC and core-valence separated ADC (CVS-ADC) up to third order.[26,27,41–44] Note that currently the algebraic expressions for the ISR in third order are not yet implemented. Therefore, the density matrices are obtained using the ADC vectores at third order with the ISR at second order. Hence, the embedding potential for FDE-ADC(3) is calculated using the MP(2) density for ρ_A^{ref}. Using this approach, it is also possible to employ other features of ADC, e.g. the wavefunction and density analysis utility `libwfa`,[45–47] or the calculation of spin-orbit coupling elements[48] which are also implemented in Q-Chem. With these tools, the direct influence of an environment on the excitations of the embedded system can be visualized via difference- and transition density analysis, attachment- and detachment density plots or generation of excited state natural orbitals.[44,46]

Currently, two different approaches are implemented to perform a FDE-ADC calculation: the supermolecular expansion (SE) and the reassembling of density matrix (RADM) approach. While the first variant is useful only for benchmark calculations, since it provides no computational savings compared to a supersystem calculation, the second variant can be used for production calculations as shown in Sec. 5.

The RADM approach is an approximation to SE.[29] Using RADM, system A is calculated twice; at first in the supermolecular basis A+B on HF level of theory obtaining the HF density matrix. This density matrix contains 4 blocks: AA, AB, BA and BB. After this, it is calculated again, now in the basis of A only on MP(2) level of theory and a separate HF-to-MP(2) difference density matrix in the basis of A is generated. The HF-to-MP(2) difference density matrix is in a following step added to the AA block of the HF density matrix of the previous calculation building a density matrix in the basis of A+B on MP(2) level of theory in the AA block and on HF level of theory on the remaining AB, BA and BB blocks,

which is called the reassembled density matrix. The environment system B is, as in SE, calculated in the supermolecular basis A+B. The subsequent calculation of the embedding potential is performed in the supermolecular basis as well. But after the embedding potential is complete, it is truncated to the AA block only. This approximation is valid, since, in the supermolecular basis, the values of the embedding potential in the off-diagonal AB and BA blocks and the values of the density matrix of A in the BB block are almost zero. (See Fig. 1) Hence, in a contraction of the density matrix of A with the embedding potential, the values in these three blocks vanish and can therefore be neglected. Consequently, the FDE-ADC calculation (step *d)*), which is the computationally most demanding step, can be performed in the basis of A only. In summary, the RADM approximation consists of an assembling of a density matrix and the truncation of the calculated embedding potential. Benchmark calculations have shown, that the errors of the FDE-ADC method in general and the error of the RADM approximation in particular are lower than the intrinsic error of the used ADC method.[29]

For the FDE-ADC calculations, a development version of Q-Chem based on version 4.4 has been used. This implementation of FDE-ADC in the module `FDEman` will be available in one of the upcoming releases of Q-Chem. Molecular pictures were captured using Avogadro 1.1.0.,[49] POV-Ray 3.7.0.RC6,[50] Jmol 13.0.14[51] and GaussView 5.0.8[52]

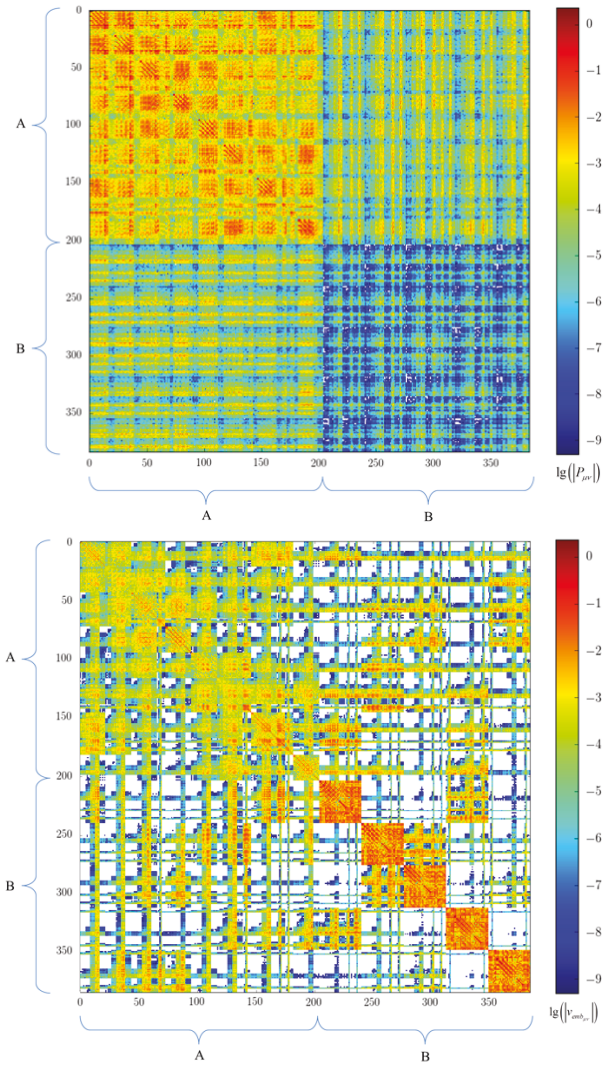

Figure 1: Graphical representation of the values of the re-assembled density matrix (top) and the total embedding potential (bottom) of the example system uracil (A) and five water molecules (B) in the basis of both subsystems (A+B). For better visibility, the decadal logarithm of the values is shown. Values below 10^{-10} are treated as zero and displayed as white in the diagram.

4 Benchmarking and Testing

4.1 Influence of the method and functional on the embedding potential

In this section, various methods for the calculation of the environment (fragment B) and the generation of the density ρ_B are tested. For this comparison, three representative model

systems were used. The first model system consists of a benzene molecule as system A and a hydrogen fluoride (HF) molecule placed side-on and almost in-plane with the benzene ring as the environment (B) ([BZ · HF]). As the second model system, a benzaldehyde molecule was used as embedded system and two water molecules forming a dimer and building a hydrogen bond to the oxygen atom of the benzaldehyde as the environment ([BA · $2\,H_2O$]). The last model system consists of a uracil molecule for A and five water molecules as B ([UC · $5\,H_2O$]). The water molecules exhibit various hydrogen bonds both among themselves and to the uracil molecule. This set of systems accounts for various interaction strengths between embedded system and environment as well as different kinds of excited states. While the first system (Benzene and HF) shows only weak and polarization based interactions, the benzaldehyde is more influenced by the environment due to the hydrogen bond in addition to the polarization of the π-system. The uracil system shows intense interactions between the core system and the environment including various hydrogen bonds. All three benchmark systems are shown in Fig. 2.

The excited states of all three systems for either the supersystem, the core system alone and in the FDE-ADC(2) approach have been studied in great detail before.[29] For all investigations, the supersystem is optimized at MP(2)/cc-pVDZ level of theory. This ensures, that no geometrical changes influence the comparison between the FDE approach and the supersystem calculation. Since the influence of the computational method, essentially the choice of xc-functional, for the environment is here in the focus of the investigation, it suffices to perform the final FDE-ADC calculation only at second-order of perturbation theory.

A large set of methods, used to calculate the environment was chosen including HF, generalized gradient approximation (GGA)-DFT (BLYP,[53,54] PBE,[55] BP86[53,56] and PW91[57]) and hybrid-DFT functionals (B3LYP,[58] BHLYP,[53,54] B5050LYP,[59] PBE0[60] and SOGGA11-X[61]). For the evaluation of the non-additive bifunctional in the embedding potential, only non-hybrid DFT functionals are allowed. Hence, the following GGA-DFT functionals were used to calculate the embedding potential: PBE,[55] BLYP,[53,54] BP86,[53,56] $G96_{corr}$[62]-$P86_{ex}$,[56]

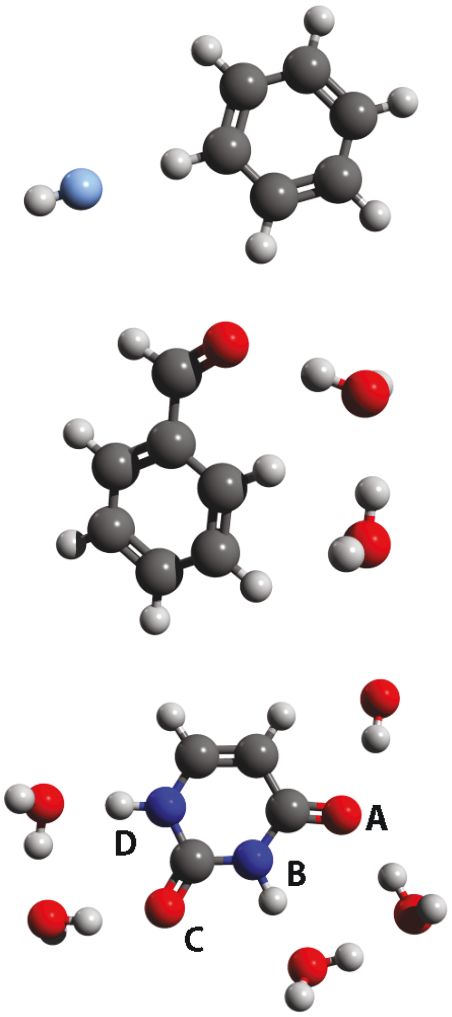

Figure 2: Molecular structures of the three test systems: benzene with a hydrogen fluoride ([BZ · HF]) (top), benzaldehyde with two water molecules ([BA · 2 H_2O])(middle) and uracil with five water molecules([UC · 5 H_2O]) (bottom).

GAM,[63] PW91[57] and SOGGA11.[61] For all calculations, the basis set cc-pVDZ[64] was used.

For all systems, the lowest five electronically excited states of the supersystem were calculated as reference at ADC(2)/cc-pVDZ level of theory. For comparison, RADM-FDE-ADC(2)/cc-pVDZ calculations were performed employing all possible combinations of the aforementioned methods for the calculation of the environment with xc-functionals for the calculation of the embedding potential. In all calculations, the Thomas-Fermi kinetic energy functional[65] was used for the kinetic energy part of the embedding potential. Since in all

cases the supersystem calculation serves as reference, deviations in excitation energies are given relative to the supersystem. Therefor, negative deviations of the excitation energy correspond to higher excitation energies in the supersystem than in the embedded system.

To summarize the key results, the test of three different systems with environment interactions ranging from weak polarization up to multiple hydrogen bonds shows only marginal dependence of the accuracy on the choice of functional used to calculate v_{emb}^{lin}. Despite the very small differences in the MAEs, some functionals can be identified to perform generally better than others in combination with ADC. The most accurate functionals used for the embedding potentials are the PBE and the PW91 functionals. The least accurate ones are the BLYP and GAM functionals. A detailed analysis of all our data is given in the supporting information. However, overall the differences are tiny and probably not relevant in practical calculations.

Regarding the theoretical method used to calculate the environment density ρ_B, the differences in accuracy are more significant. In general, hybrid functionals and HF itself perform better than functionals without exact exchange. This tendency becomes particularly visible when strong interactions between the embedded system and the environment play a role. In these cases, the accuracy depends clearly on the amount of HF exchange, the more the better. Additionally, it seems not advantageous to apply the same xc-functional for the calculation of ρ_B and for the embedding potential. In fact, it turns out HF has the smallest MAE when ADC is used for the embedded system. The MAEs for all investigated combinations of method to calculate ρ_B and xc-functional used in the embedding potential are summarized in Fig. 3. A possible explanation for the observed trend is, that also the density of the embedded system, which is calculated using MP(2) level of theory, is largely based on HF theory. This is also the case in the supermolecular reference calculation. Hence, both densities "match" best, when both are calculated using the same underlying theoretical model, i.e. HF, as in the supermolecular approach.

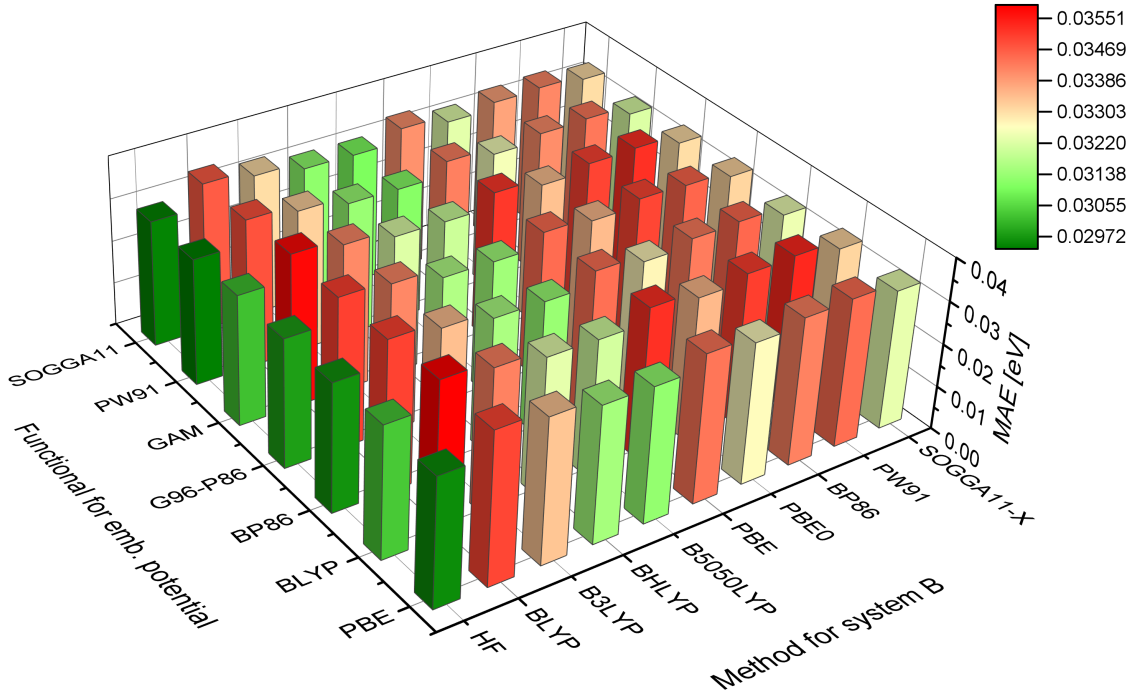

Figure 3: Mean absolute errors (MAE) of the environment induced excitation energy shifts of the computed states of all three investigated system (benzene + hydrogen fluoride, benzaldehyde + two water molecules and uracil + five water molecules) for all investigated combinations of method to calculate the environment density and the functional to calculate the non-electrostatic part of the embedding potential.

4.2 Benchmark of FDE-ADC(3)

In this chapter, the first results for the combination of frozen density embedding (FDE) with the algebraic-diagrammatic construction scheme of the polarization propagator of third order (ADC(3)) are presented. Analogously to the previously demonstrated variant FDE-ADC(2),[29] this new method is referred to as FDE-ADC(3). Accordingly to the benchmark of FDE-ADC(2), the same test set of *1)* [BZ·HF], *2)* [BA·2 H_2O] and *3)* [UC·5 H_2O] will be employed (Fig. 2). As before, the geometries have been optimized at MP(2)/cc-pVDZ level of theory for the supersystem and used for all calculations to exclude energy differences due to geometry differences. The supersystems and the isolated core systems (A) were investigated at ADC(3)/6-311++G**[66–68] level of theory. For the FDE-ADC(3) calculations, the reassembling of density matrix approximation (RADM) and the same basis set 6-311++G**

was used, since previous studies showed an improved accuracy for FDE-ADC when diffuse basis sets are employed.[29] Only in [BA $\cdot$ 2 H_2O], the aug-cc-pVDZ basis set was chosen due to convergence issues in the supersystem calculation using the 6-311++G** basis set. The RADM approach was chosen, since this is the variant capable of performing productive calculations of larger systems. The HF method was chosen for the calculation of the environment density ρ_B and the PBE functional for the non-electrostatic part of the embedding potential since this combination exhibits the smallest error as shown in the previous Section **??**.

Note that the supersystem calculation is always taken as reference for both isolated and FDE-ADC(3) results. Hence, solvatochromic shifts and deviations of FDE-ADC from the supersystem results are calculated as $\omega_{isol} - \omega_{sup}$ and $\omega_{FDE-ADC} - \omega_{sup}$, respectively. As a consequence, a negative value indicates a larger excitation energy in the supersystem (blue shift). The same holds for oscillator strengths.

4.2.1 Benzene and hydrogen fluoride

Starting again with the weakly interacting system [BZ $\cdot$ HF]. At first, [BZ $\cdot$ HF] and isolated benzene are investigated. Next, a FDE-ADC(3) calculation is performed and the results are compared to the supermolecular calculation. While the occupied frontier orbitals, i.e. the highest occupied molecular orbital (HOMO) and HOMO-1 are typical π orbitals, the corresponding unoccupied frontier orbitals, i.e. the lowest unoccupied molecular orbital (LUMO) and LUMO+1, are not necessarily the corresponding π^* orbitals. Due to the diffuse basis functions, Rydberg and various other types of virtual orbitals are present compared to calculations using basis sets without diffuse basis functions. Therefore, the corresponding π^* to the HOMO and HOMO-1 are LUMO+7 and LUMO+8 in the supermolecular calculation. The LUMO+1 for example is a Rydberg orbital (R) located in the benzene ring plane opposite to the hydrogen fluoride.

The four energetically lowest electronically excited states of [BZ $\cdot$ HF] were calculated. The S_1- and S_4 state are ($\pi \mapsto \pi^*$) transitions, while S_2 and S_3 are Rydberg states. A

detailed analysis of the excitations is given in Table 1. In isolated benzene, HOMO and HOMO-1 have π character, while LUMO and LUMO-1 instead are Rydberg orbitals. The energetically lowest π^* orbitals are the LUMO+6 and LUMO+7. For isolated benzene, also the lowest four excitations were calculated. The S_1- and S_4 states show ($\pi \mapsto \pi^*$) character, the S_2- and S_3 states are Rydberg states. A more detailed analysis is given in Table 1. However, it is noticeable, that in the calculations employing ADC(3)/6-311++G** the solvatochromic shifts differ from the calculations at ADC(2)/cc-pVDZ level. While using the latter a solvatrochromic blue shift due to hydrogen fluoride could be observed for states S_1 to S_4 (($\pi \mapsto \pi^*$) transitions),[29] two ($\pi \mapsto \pi^*$) excited states show a small red shift at ADC(3)/6-311++G** level of theory.

Table 1: Excitation energies, oscillator strengths and orbital transitions for the four energetically lowest electronically excited singlet states of isolated benzene, [BZ · HF] using the supermolecular ADC(3) and FDE-ADC(3) methods. Orbital transitions with >10 % are given.

	Excitation Energies [eV] and Osc. Str.			Orb. Trans.	Weight [%]		
state	Iso.[a]	Sup.[b]	FDE[c]	H+x $\mapsto$ L+y[d]	Iso.[a]	Sup.[b]	FDE[c]
S_1	5.049 (0.0000)	5.050 (0.0001)	5.049 (0.0001)	0 $\mapsto$ 6 ($\pi \mapsto \pi^*$)	36.8	37.5[e]	37.5
				-1 $\mapsto$ 7 ($\pi \mapsto \pi^*$)	36.8	34.8[e]	35.4
S_2	6.369 (0.0000)	6.292 (0.0008)	6.293 (0.0007)	0 $\mapsto$ 0 ($\pi \mapsto R$)	79.2	18.0	27.3
				0 $\mapsto$ 1 ($\pi \mapsto R$)	-	57.8	51.9
S_3	6.369 (0.0000)	6.310 (0.0000)	6.312 (0.0000)	-1 $\mapsto$ 0 ($\pi \mapsto R$)	79.2	18.0	27.5
				-1 $\mapsto$ 1 ($\pi \mapsto R$)	-	56.1	50.4
S_4	6.405 (0.0000)	6.396 (0.0000)	6.397 (0.0001)	-1 $\mapsto$ 6 ($\pi \mapsto \pi^*$)	42.1	42.0[e]	42.1
				0 $\mapsto$ 7 ($\pi \mapsto \pi^*$)	42.1	40.7[e]	41.5

[a] isolated benzene
[b] supermolecular ADC(3)
[c] RADM-FDE-ADC(3)
[d] H = HOMO, L = LUMO, R = Rydberg-type orbital
[e] An orbital localized at the hydrogen fluoride is neglected in counting (see text)

In the RADM-FDE-ADC(3) calculation, the hydrogen fluoride is modeled by virtue of the embedding potential. The resulting orbitals look qualitatively identical to the ones obtained in the isolated benzene calculation. However, since also in the supermolecular calculation

the orbitals localized at the benzene did not show any difference to the isolated benzene orbitals, this result is not unexpected. In the supermolecular calculation, additional orbitals located at hydrogen fluoride are included, which are by set-up not included in the other calculations. For ease of comparison, this is taken care of in the orbital numbering, and the orbital numbering of the supermolecular calculation is generally adapted.

Overall, the FDE-ADC(3) calculation shows almost quantitative agreement with the supermolecular calculation. The S_1 and S_4 state exhibit ($\pi \mapsto \pi^*$) transition character, the S_2 and S_3 states are identified as Rydberg states (Table. 1). A diagrammatic representation of the absorbance shift induced by the environment, i.e. the difference between supermolecular calculation and isolated benzene as well as an illustration of the accuracy of the FDE-ADC(3) method in comparison with the supermolecular calculation is given in Fig. 4.

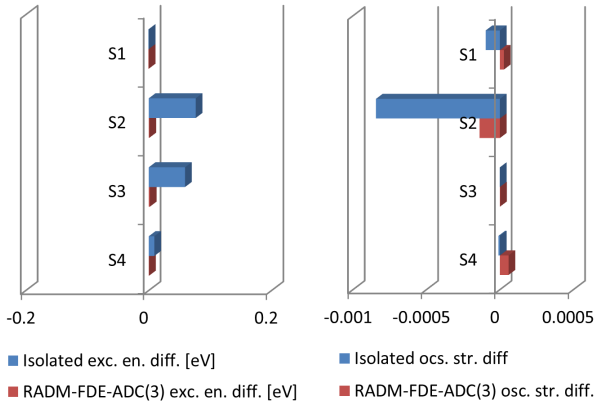

Figure 4: Analysis of the accuracy of FDE-ADC(3) for [BZ·HF]. Excitation energy difference (left) and oscillator strength difference (right) of the isolated benzene to the supersystem (blue) and the FDE-ADC(3) calculation using the RADM approximation to the supersystem (red). The blue bars correspond to the absorbance shift due to the influence of the environment on the excitation energies and oscillator strengths (solvatochromic shift) while the red bars indicate the accuracy of the FDE-ADC(3) calculation in comparison with the ADC(3) supersystem calculation.

The largest deviation in excitation energies is smaller than 0.002 eV and about 0.0001 for oscillator strengths when the FDE-ADC(3) calculation is compared to the supermolecular ADC(3) calculation. The mean absolute error (MAE) of all four states in excitation energies is 0.001 eV and 0.0001 for oscillator strengths, respectively.

4.2.2 Benzaldehyde with two water molecules

Analogously to the previous system, FDE-ADC(3) has been tested for [BA · 2 H_2O]. In both the supermolecular and the isolated benzene calculation, the HOMO, HOMO-1 and HOMO-2 exhibit π, π and n character, respectively. However, due to the chosen diffuse basis set, corresponding π^* orbitals can be found as LUMO+3 in [BA · 2 H_2O] and LUMO+4 in the isolated benzaldehyde calculation. Obviously, some orbitals changed their energetic order due to the effect of the two water molecules. Further important π^* orbitals arise as LUMO+7 and LUMO+8 in isolated benzene and as LUMO+9 in [BA · 2 H_2O]. The occupied orbitals HOMO and HOMO-1 are reoriented when including the water molecules. (See Fig. 5)

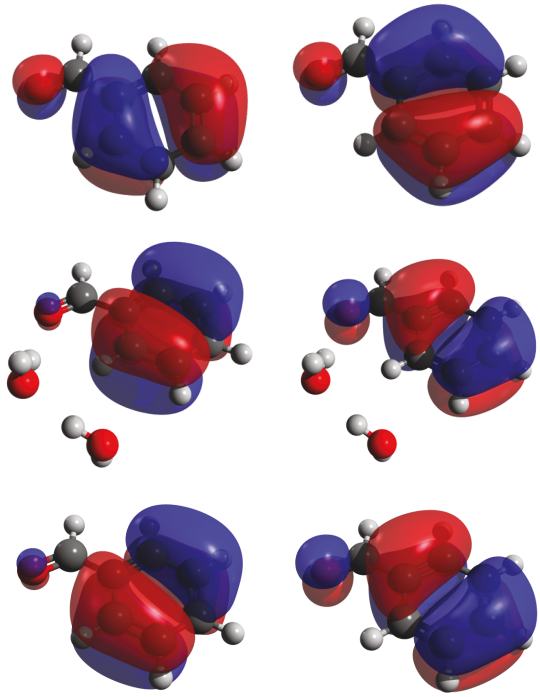

Figure 5: HOMO (left side) and HOMO-1 (right side) of isolated benzaldehyde (top), of [BA · 2 H_2O] calculated with supermolecular ADC(3) (middle) and with FDE-ADC(3) (bottom).

The five energetically lowest excited states have been calculated both for [BA · 2 H_2O] and isolated benzaldehyde. However, in none of these systems and independent from the chosen basis set, the calculations of the fourth excited state (S_4) did not converge. In both cases, the first excited state exhibits ($n \mapsto \pi^*$) excitation character while the states S_2, S_3 and S_5 exhibit

local ($\pi \mapsto \pi^*$) transition character. The solvatochromic shift for benzaldehyde is -0.24 eV for the ($n \mapsto \pi^*$) excitation and between 0.1 eV and 0.18 eV for the ($\pi \mapsto \pi^*$) excitations. A detailed overview of the calculated excited states is given in Table 2. The reorientation of the HOMO and HOMO-1 prevents a direct mapping of the corresponding transitions between isolated benzaldehyde and the supermolecular calculation. But since the orbitals are still of the same type and form and also the orbital energies are quite similar, this change does not affect the character of the excited states themselves.

Table 2: Excitation energies, oscillator strengths and main orbital transitions (> 10 %) for the five energetically lowest electronically excited singlet states[a] of isolated benzaldehyde and [BA·2 H_2O] using supermolecular ADC(3) and FDE-ADC(3) with the RADM approximation.

	Excitation Energies [eV] and Osc. Str.			Orb. Trans.	Weight [%]		
state[a]	Iso.[b]	Sup.[c]	FDE[d]	H+x $\mapsto$ L+y[e]	Iso.[b]	Sup.[c]	FDE[d]
S_1	3.827 (0.0002)	4.063 (0.0003)	4.038 (0.0002)	-2 $\mapsto$ 3 ($n \mapsto \pi^*$)	63.4[f]	63.5	65.5
S_2	6.369 (0.0110)	4.454 (0.0188)	4.476 (0.0157)	0 $\mapsto$ 3 ($\pi \mapsto \pi^*$)	19.0[f,g]	53.1[g]	52.0
				-1 $\mapsto$ 3 ($\pi \mapsto \pi^*$)	36.2[f,g]	5.2[g]	7.6
				-1 $\mapsto$ 8 ($\pi \mapsto \pi^*$)	-	-	12.9
S_3	6.369 (0.2827)	5.160 (0.2878)	5.207 (0.3006)	-1 $\mapsto$ 3 ($\pi \mapsto \pi^*$)	24.0[f,g]	66.3[g]	66.0
				0 $\mapsto$ 3 ($\pi \mapsto \pi^*$)	54.0[f,g]	8.7[g]	12.1
S_5	6.405 (0.3487)	6.368 (0.3084)	6.399 (0.2874)	0 $\mapsto$ 8 ($\pi \mapsto \pi^*$)	19.3[g]	-	6.1[h]
				0 $\mapsto$ 3 ($\pi \mapsto \pi^*$)	-	16.5[g]	17.1[h]
				-1 $\mapsto$ 3 ($\pi \mapsto \pi^*$)	19.0[g,f]	-	4.5[h]
				0 $\mapsto$ 7 ($\pi \mapsto \pi^*$)	13.8[g,h]	-	-
				-1 $\mapsto$ 8 ($\pi \mapsto \pi^*$)	10.0[g,h]	13.8[g,h]	36.7[h]
				-1 $\mapsto$ 12 ($\pi \mapsto \pi^*$)	-	13.5[g,h]	-

[a] Please note that the S_4 state did not converge in all calculations.
[b] isolated benzaldehyde
[c] supersystem ADC(3) calculation
[d] RADM-FDE-ADC(3)
[e] H = HOMO, L = LUMO
[f] A Rydberg orbital is neglected in counting, i.e. LUMO indices reduced by 1 to match the numbers
[g] Since HOMO and HOMO-1 are differently oriented in Iso. [b] and Sup.[c] the energetic numbering might not necessarily match.
[h] Since various Rydberg orbitals change their energetic ordering, orbital indices might not match

In the FDE-ADC(3) calculations, the influence of the environment is very well repro-

duced. Also the reorientation of the HOMO and HOMO-1 is reproduced in the FDE-ADC(3) calculation, (Fig. 5). The MAE in excitation energies is 0.031 eV and in oscillator strength 0.0092. The character of the excited states, compared to $[BA \cdot 2\,H_2O]$, is retained. While S_1 has an $(n \mapsto \pi^*)$ character, S_2, S_3 and S_5 state exhibit $(\pi \mapsto \pi^*)$ character. A diagrammatic representation of the accuracy of the FDE-ADC(3) calculation for $[BA \cdot 2\,H_2O]$ is given in Fig 6

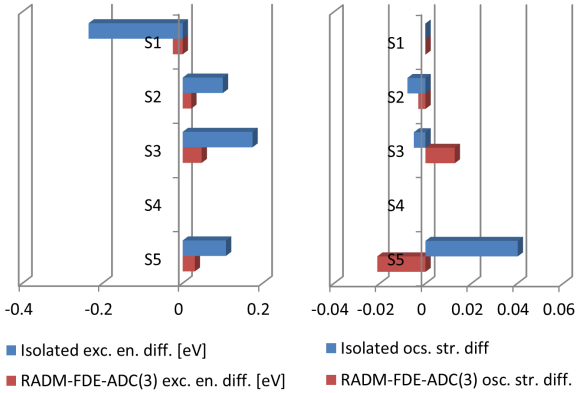

Figure 6: Analysis of the accuracy of FDE-ADC(3) of $[BA \cdot 2\,H_2O]$. Excitation energy difference (left) and oscillator strength difference (right) of the isolated benzaldehyde to the supersystem (blue) and the FDE-ADC(3) calculation using the RADM approximation to the supersystem (red). The blue bars correspond to the solvatochromic shift while the red bars indicate the accuracy of the FDE-ADC(3) calculation in comparison with the supermolecular ADC(3) calculation.

4.2.3 Uracil with five water molecules

For the last benchmark system, $[UC \cdot 5\,H_2O]$, the same analysis has been performed. HOMO and HOMO-1 in both the $[UC \cdot 5\,H_2O]$ and the isolated uracil exhibit π character. HOMO-2 and HOMO-3 are n orbitals localized at the oxygen atoms. Calculation of the five energetically lowest excited states of $[UC \cdot 5\,H_2O]$ reveals four $(\pi \mapsto \pi^*)$ transitions i.e. S_1, S_3, S_4, and S_5. The S_2 state exhibits $(n \mapsto \pi^*)$ transition character. In contrast, in isolated uracil, the S_1 state is an $(n \mapsto \pi^*)$ state and the states S_2 to S_4 are $(\pi \mapsto \pi^*)$ states. For this system, the molecular orbital picture is insufficient to analyze the character of the excited states properly, since many orbital transitions contribute to the excitation and the orbitals

themselves change both in form and energetic order between isolated uracil and $[UC \cdot 5\,H_2O]$. Therefore, natural transition orbitals (NTOs)[69–71] have been calculated and analyzed to characterize the excited states. These NTOs reveal the S_1 state of isolated uracil to correspond to the S_2 state of $[UC \cdot 5\,H_2O]$ while the S_1 state of the supersystem corresponds to the S_2 state of isolated uracil. The S_3 state is identical in both cases, while the S_4 and S_5 state in $[UC \cdot 5\,H_2O]$ exhibit a different character than any of the calculated states of isolated uracil. These states are energetically lowered by the environment. An electronic state of $[UC \cdot 5\,H_2O]$ corresponding to the S_4 state of isolated uracil could not be identified. To facilitate comparison of corresponding states, each state is assigned to a Greek letter based on its character and not on its energetic order, (see Table 3).

Table 3: Excitation energies and oscillator strengths for the five energetically lowest electronically excited singlet states of isolated uracil, $[UC \cdot 5\,H_2O]$ at supermolecular ADC(3) level as well as at FDE-ADC(3) level with the RADM approximation.

	Excitation Energies [eV] and Osc. Str.			Transition Character		
state	Iso.[a]	Sup.[b]	FDE[c]	Iso.[a]	Sup.[b]	FDE[c]
S_1	5.015 (0.0000)	5.123 (0.2534)	5.199 (0.2235)	$(n \mapsto \pi^*)$ (α)	$(\pi \mapsto \pi^*)$ (β)	$(\pi \mapsto \pi^*)$ (β)
S_2	5.299 (0.2454)	5.764 (0.0000)	5.668 (0.0000)	$(\pi \mapsto \pi^*)$ (β)	$(n \mapsto \pi^*)$ (α)	$(n \mapsto \pi^*)$ (α)
S_3	5.716 (0.0027)	6.193 (0.0130)	6.208 (0.0132)	$(\pi \mapsto \pi^*)$ (γ)	$(\pi \mapsto \pi^*)$ (γ)	$(\pi \mapsto \pi^*)$ (γ)
S_4	6.330 (0.0341)	6.383 (0.1014)	6.456 (0.0957)	$(\pi \mapsto \pi^*)$ (δ)	$(\pi \mapsto \pi^*)$ (ϵ)	$(\pi \mapsto \pi^*)$ (ϵ)
S_5	-	6.627 (0.2207)	6.631 (0.2069)	-	$(\pi \mapsto \pi^*)$ (ζ)	$(\pi \mapsto \pi^*)$ (ζ)

[a] isolated uracil
[b] supermolecular ADC(3)
[c] RADM-FDE-ADC(3)

In the FDE-ADC(3) calculation, the effect of the environment onto the embedded system is generally well reproduced. HOMO and HOMO-1 exhibit π character, the HOMO-2 and HOMO-3 show n character and each is localized on one oxygen atom. The excited states have the same character and energetic order as in the supermolecular calculation. With an MAE of 0.053 eV for excitation energies and 0.01 for oscillator strengths also the excited state properties are in good agreement with the supermolecular calculation. This is displayed in Fig. 7. However, since the S_5 state did not converge in the isolated uracil calculation

and the S_4 state differs from the S_4 state in the supermolecular calculation, these values are excluded from the comparison. Additionally, since the energetic order of the states changes from isolated uracil to $[UC \cdot 5\,H_2O]$, the comparison is based on the character of the states and the assingment has been done according to the supermolecular results.

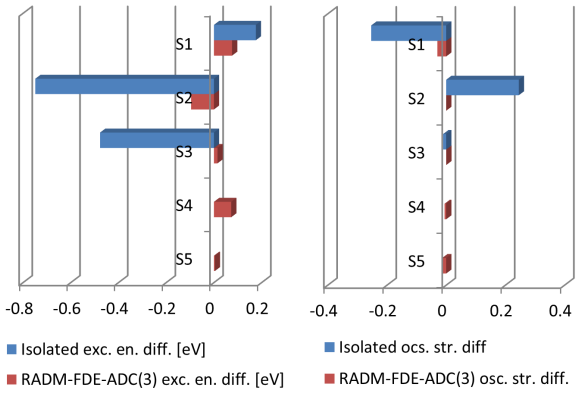

Figure 7: Analysis of the accuracy of FDE-ADC(3) for $[UC \cdot 5\,H_2O]$. Excitation energy difference (left) and oscillator strength difference (right) of the isolated uracil to the supersystem (blue) and the FDE-ADC(3) calculation using the RADM approximation to the supersystem (red). The blue bars correspond to the solvatochromic shift while the red bars indicate the accuracy of the FDE-ADC(3) calculation in comparison to the supermolecular ADC(3) calculation. The results for states S_4 and S_5 of isolated uracil are excluded.

5 Representative Applications of FDE-ADC

After benchmarking FDE-ADC(3) in the previous section, the potential of the FDE-ADC method shall be demonstrated at three representative examples, which comprise computations of larger systems. For these, supermolecular calculations at ADC(3) level are no longer feasible and instead the RADM approximation has to be employed. In the first example, the excited states of benzoquinone solvated in methanol are investigated. In the second example, the photoswitch spiropyran dissolved in water is analyzed and compared to QM/MM calculations from the literature.[72] In the third example, the core-excited states of $CO@C_{60}$, a CO molecule caught in a C_{60} fullerene, are calculated using the core-valence separated FDE-CVS-ADC method. The different influence of a C_{60}-cage on the core excitations in

carbon monoxide are investigated.

5.1 Excited states of para-benzoquinone in methanol

To simulate para-benzoquinone in methanol solution, a para-benzoquinone molecule was surrounded by 42 methanol molecules. Benzoquinone was chosen as example because it is a symmetric molecule of moderate size, has a delocalized π-electron system, can act as hydrogen bond acceptor and exhibits low-lying electronically excited states with both single- and double excitation character. Therefore, a quantum chemical method including doubly excited configurations in more than zeroth order of perturbation theory, like ADC(3), is needed to describe the excitations properly.[27] Since benzoquinone is soluble in moderately polar solvents, methanol was chosen as environment. The supersystem is shown in Fig. 8.

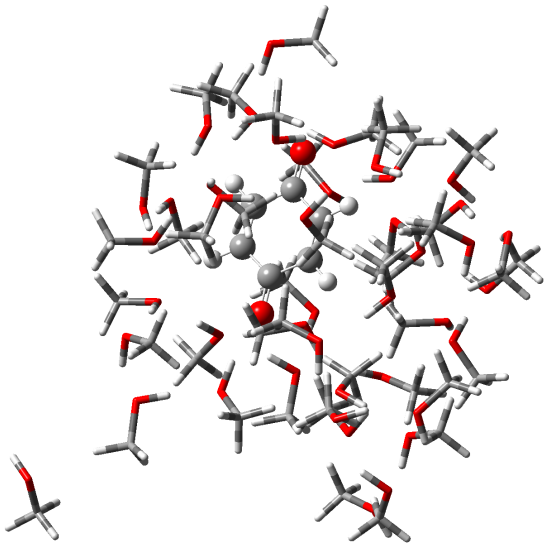

Figure 8: Supersystem of benzoquinone (balls and sticks, embedded system (A)) and 42 methanol molecules (environment (B)).

Isolated benzoquinone was optimized at MP(2) / cc-pVTZ level of theory. This geometry serves as the reference for gas phase calculations. Additionally, the supersystem of benzoquinone and 42 methanol molecules placed around the benzoquinone was fully optimized at DFT / ωB97X-D3[73] / 6-31G* level of theory. This structure was used for the

investigations of the effects of the environment. The obtained structure is just one possible representative simulating an environment, and for the purpose here, it is not necessary to be the energetically lowest possible structure. The two energetically lowest excited states of p-benzoquinone are investigated at ADC(3)/6-311G** level of theory for the two isolated benzoquinone structures i.e. one optimized at MP(2) level in the gas phase and the other cut out of the methanol environment, and at FDE-ADC(3)/6-311G** level of theory for the supersystem. For the FDE-ADC(3) calculation, the RADM approximation was used, the density of the environment was calculated at HF level of theory and the non-electrostatic part of the embedding potential was calculated employing the PBE functional. In the gas phase, these states are with excitation energies of 2.840 eV and 2.999 eV close in energy. Both are ($n \mapsto \pi^*$) states each containing transitions from both n orbitals localized at the oxygen atoms. Therefore, both excited states have practically no oscillator strength. The excitation character is visualized by attachment and detachment densities (Fig. 9). The detachment density is that part of the total electron density that is removed upon excitation and replaced by the attachment density. In combination, they unambiguously characterize the electronic transition.

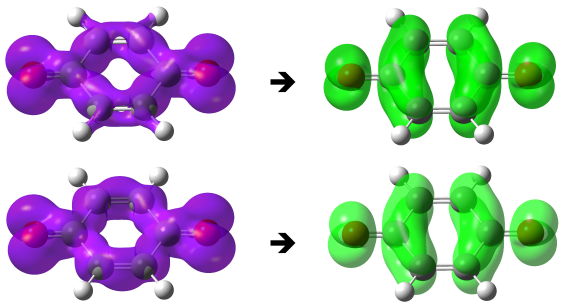

Figure 9: Detachment (left) and attachment (right) densities of the S_1 (top) and S_2 state of isolated gas phase benzoquinone.

A very similar excitation pattern is obtained for the supersystem-optimized isolated benzoquinone structure. Both S_1 and S_2 exhibit ($n \mapsto \pi^*$) transition character. Since the geometry is slightly different, also the excitation energies vary slightly and correspond to 2.893 eV and 3.077 eV for S_1 and S_2, respectively. The oscillator strength of both states is

still zero, and also the attachment and detachment densities are practically identical to the gas phase picture. However, they are slightly distorted due to the solvation-induced changes in the geometry. (Figure S1 in supporting information)

A different picture is obtained when the environment is included via FDE. While the excitation energy of the first excited state is almost identical to the isolated calculation in the supersystem-optimized geometry, the excitation energy of the second excited state is increased by about 0.23 eV. Although both excited states are still ($n \mapsto \pi^*$) states, they are now localized on one of the oxygen atoms each. The environment induces a separation and localization of the two excited states. This is nicely identified by the attachment- and detachment densities (Fig. 10).

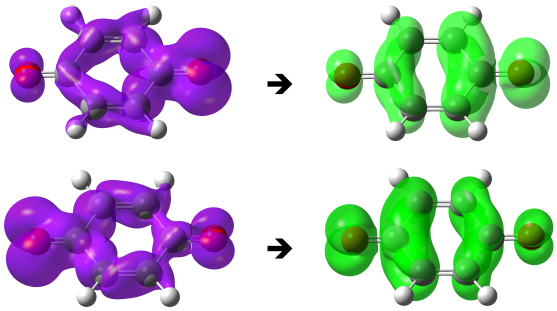

Figure 10: Detachment (left) and attachment (right) densities of the S_1 (top) and S_2 state (bottom) of benzoquinone embedded in 42 methanol molecules at FDE-ADC(3) level of theory.

5.2 Transition densities of spiropyran in water

Spiropyran is a molecular photoswitch, which undergoes a ring-opening and isomerization reaction upon irradiation with UV-light.[74–76] The photoisomerization process has been investigated spectroscopically using femtosecond vis-pump/vis- and IR-probe spectroscopy[77,78] and also previous QM/MM calculations on spiropyran in water demonstrated an only small influence of water on the vertical excitations and photochemistry of spiropyran.[72] The energetically lowest excited states have been characterized as "bright" and "dark" state indicating the difference in oscillator strengths. Occupying the bright state leads to a ring-opening reac-

tion to merocyanine. These two important excited states could be identified in the presence of the water environment as well.[72] This finding shall here be verified using FDE-ADC.

A supersystem of spiroypran and 100 water molecules arranged in at least two solvation shells around spiropyran was created and fully optimized at DFT/ωB97X-D3/6-31G* level of theory. This structure is used for the calculation of vertical excitation energies of isolated spiropyran as well as of the embedded system using FDE-ADC.

The calculations of the excited states have been performed at ADC(2)/cc-pVDZ and FDE-ADC(2)/cc-pVDZ level of theory. For the FDE-ADC(2) calculation, the environment density was calculated using HF and the non-electrostatic part of the embedding potential was calculated using the PBE functional. The geometry of the supersystem is shown in Fig. 11

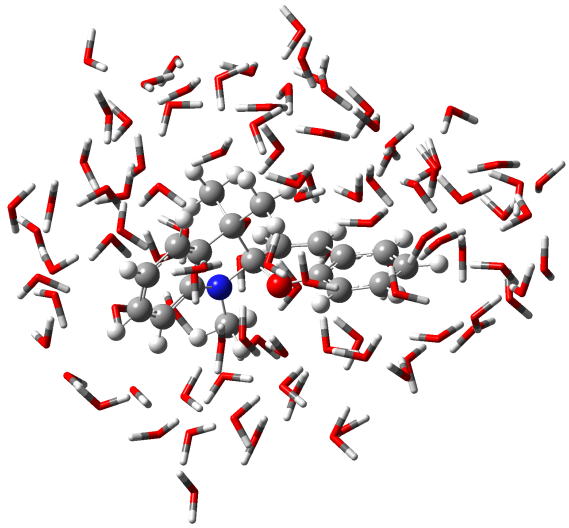

Figure 11: Supersystem of spiropyran (balls and sticks, embedded system (A)) surrounded by 100 water molecules (environment (B)).

The two energetically lowest excited states were calculated and analyzed using natural transition orbitals (NTOs).[69–71] NTOs are orbitals specific for one excitation and describe the electron transition itself. NTOs always come in pairs, one representing the particle, the other representing the hole. Both share the same eigenvalue which corresponds to the contribution of this pair to the total excitation. Although it is mathematically not fully

correct, for the sake of simplicity, the nomenclature used for molecular orbitals is also applied here. Therefore, the hole NTO exhibiting the highest eigenvalue is labeled "highest occupied natural transition orbital" (HONTO) and the corresponding particle NTO sharing the same eigenvalue is labeled "lowest unoccupied natural transition orbital" (LUNTO). The NTO pairs exhibiting lower eigenvalues follow the same scheme (HONTO-1, LUNTO+1,...).

In isolated spiropyran, the S_1 and S_2 states exhibit excitation energies and oscillator strengths of 4.172 eV (0.0506) and 4.434 eV (0.0084), respectively. Analyzing the corrsponding NTOs, the S_1 state can be identified as local ($\pi \mapsto \pi^*$) transition on the benzopyran moiety and the S_2 state as a charge-transfer state from the indoline moiety to the benzopyran side. The leading NTO pairs for both the S_1 and S_2 states are shown in the supporting information. They are qualitatively identical to the NTOs shown in Fig. 12.

In the FDE-ADC(2) calculation, the excitation energy of the S_1 state is increased while the excitation energy of the S_2 state decreases. The excitation energies and oscillator strengths of S_1 and S_2 are now 4.222 eV (0.0438) and 4.265 eV (0.0096), respectively, however their transition character is not changed compared to isolated spiropyran. The leading NTO pairs of the two energetically lowest excited states are given in Fig. 12.

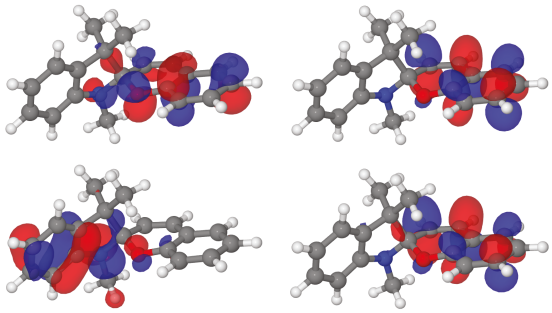

Figure 12: HONTO (left) and LUNTO (right) of the S_1 (top) and S_2 (bottom) state of spiropyran calculated with FDE-ADC(2).

These results confirm previous studies of spiropyran in water on QM/MM level of theory.[72] The water environment shifts the vertical excitation energies slightly but does not affect the photochemistry of spiropyran significantly, it still functions as photoswitch in water.

5.3 Core excited states of carbon monoxide in fullerene

For the computation of core-excited states, the core-valence separation can be employed within ADC schemes and an efficient computer program has recently been developed.[41–44] This facilitates the calculation of energetically high lying core-excited states dramatically.

In this section the influence of a C_{60} cage on the core excitations of a carbon monoxide incorporated in C_{60} are demonstrated. For that purpose, CO@C_{60} was created and fully optimized at DFT/ωB97X-D3/6-31G* level of theory. The system is shown in Fig. 13.

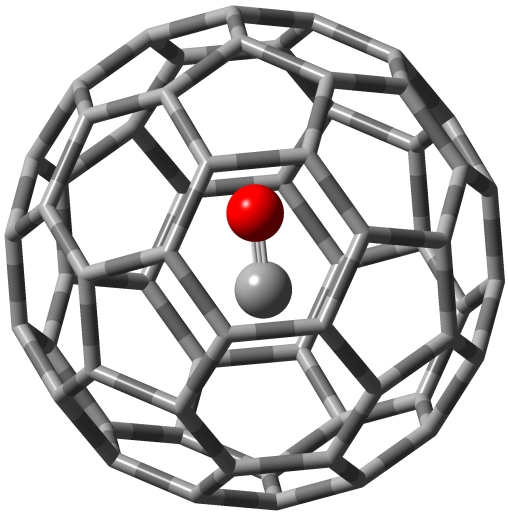

Figure 13: CO@C_{60}, drawn as balls and sticks (embedded system (A)) and C_{60} molecule (environment (B)).

For comparison the five energetically lowest (C_{1s})-core excited states were calculated at CVS-ADC(2)-x/6-311++G** level of theory for isolated CO. The core-excited states S_1^c to S_5^c exhibit the following character: ($C_{1s} \mapsto \pi^*$), ($C_{1s} \mapsto \pi^*$), ($C_{1s} \mapsto \sigma^*$), ($C_{1s} \mapsto \pi^*$) and ($C_{1s} \mapsto \pi^*$), respectively. The corresponding excitation energies are given in Tab. 4. S_1^c and S_2^c as well as S_4^c and S_5^c are degenerate.

Employing the FDE-ADC approach for including the effect of C_{60}, the five energetically lowest core excited states were recalculated including the embedding potential obtained from a HF calculation for the electron density of C_{60} and the PBE functional for the non-electrostatic part of v_{emb}^{lin} using the RADM approximation. Including the environment in

the calculation of core excited states via FDE-CVS-ADC shows only small influences. All calculated C_{1s}-core excited states are very similar to the results obtained for isolated CO regarding energies as well as properties and characters. This is verified by difference density analysis. The largest energetic shift is observed for the S_3^c state with about 0.2 eV. The excitation character of all five calculated states is retained. However, since C_{60} breaks the symmetry of CO, S_1^c and S_2^c as well as S_4^c and S_5^c are not fully degenerate any more. In Table 4, the excitation energies and oscillator strengths for the five energetically lowest C_{1s}-core excitations are given.

Table 4: Excitation energies and oscillator strengths of the five energetically lowest C_{1s}-core excitations of isolated CO and CO@C_{60}using the FDE-CVS-ADC(2)-x method.

	Core excited states C 1s	
state	Iso. CVS-ADC(2)-x	FDE-CVS-ADC(2)-x
S_1	287.730 (0.071)	287.656 (0.073)
S_2	287.730 (0.071)	287.659 (0.073)
S_3	293.299 (0.004)	293.493 (0.003)
S_4	294.577 (0.010)	294.593 (0.006)
S_5	294.577 (0.010)	294.628 (0.007)

The difference density plots for the core excited states of CO@C_{60} obtained using the FDE-CVS-ADC method are qualitatively identical to the ones obtained for isolated CO. Note, that in the core excited difference density plots most of the change in electron density is due to orbital relaxation effects.[44] The difference densities for the five energetically lowest C_{1s}-core excited states S_1^c to S_5^c obtained using FDE-CVS-ADC(2)-x are shown in Fig. 14

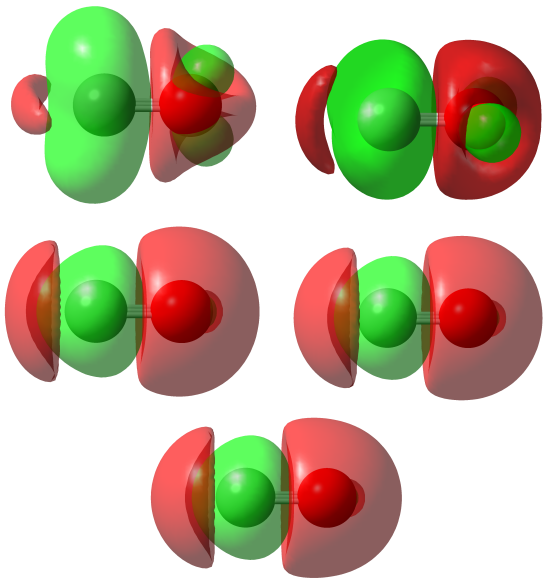

Figure 14: C_{1s}-core excited difference density plots of S_1^c (top left), S_2^c (top right), S_3^c (middle left), S_4^c (middle right) and S_5^c (bottom) of $CO@C_{60}$ calculated using FDE-CVS-ADC(2)-x. The difference density plots for isolated CO are practically identical.

6 Summary and Conclusion

In this article, the implementation and application of the FDE-ADC approach up to third order of perturbation theory based on the combination of linearized FDET and ADC is presented. A previously published interface-based approach using both Molcas and Q-Chem[29] has been improved to a user-friendly Q-Chem only implementation. Beyond a more straightforward application of FDE-ADC in general, this also enables the use of additional features already contained in the `adcman` module, for example the core-valence separation (CVS) and wave-function analysis tools (WFA). The implementation comprises now all available levels of ADC up to third order. The embedding scheme can be carried out in two different molecular orbital expansions. The supermolecular expansion expresses the embedding potential in the basis of both embedded system and environment and is only intended for benchmarking purposes of FDE-ADC. For productive calculations the RADM approach is available, in which the embedding potential is expressed in the basis of the embedded system only.

In first tests and benchmarks, the choice of method used to calculate the environment density ρ_B using HF and DFT with various functionals and the choice of functional used to calculate the non-electrostatic part of the embedding potential was evaluated. Fur this purpose, three benchmark system: 1) benzene with one hydrogen fluoride molecule [BZ $\cdot$ HF] 2) benzaldehyde with a hydrogen-bonded water dimer [BA $\cdot$ 2 H_2O] and 3) uracil with 5 hydrogen-bonded water molecules [UC $\cdot$ 5 H_2O] have been employed. In summary, almost no dependence of the results on the employed functional for the calculation of the embedding potential could be observed. For the choice of the method used to calculate the environment, it could be seen that HF performs best and that the MAE is reduced with increasing amount of HF exchange. Possibly this behavior owes to the better match of a HF based density for the environment with the HF/MP2 based density of the embedded system.

The same test systems were used to benchmark the accuracy of the new FDE-ADC(3) method by comparison to supermolecular calculations at ADC(3) level of theory . For the

FDE-ADC(3) calculations, HF and the functional PBE were chosen for the calculation of the environment density and the non-electrostatic interaction, respectively. In all cases, the five energetically lowest excited states were calculated. The MAEs for the three systems are 0.001 eV for excitation energies and 0.0001 for oscillator strength for [BZ·HF], 0.031 eV (EE) and 0.0093 (OS) for [BA · $2\,H_2O$] and 0.053 eV (EE) and 0.01 (OS) for [UC · $5\,H_2O$]. This demonstrates the accuracy of the introduced FDE-ADC(3) method for very weak dispersive system-environment interactions up to very strong interactions via multiple hydrogen bonds.

In the last section three representative applications of FDE-ADC on larger systems are presented. The splitting of two nearly degenerate ($n \mapsto \pi^*$) excited states of benzoquinone due to a methanol environment is analyzed. The influence of a water environment onto the excited states of the photoswitch spiropyran is investigated, and the influence of the C_{60} cage onto the C_{1s}-core excited states of CO in CO@C_{60} is computed using FDE-CVS-ADC. In all three cases, the specific excitation properties are visualized by transition- and difference density analyses.

In a future extension of the FDE-ADC implementation, the so called monomer expansion (ME) will be implemented. In this approach, each subsystem is calculated in its own molecular orbital basis only and thus the error introduced by the truncation of the embedding potential as done in RADM is omitted.

In summary, the presented FDE-ADC implementation gives access to include explicit environment influences on the excitation process. Exhibiting an error lower than the intrinsic error of the used ADC method[27] makes FDE-ADC to a reliable "black box" method for embedded systems in extended environments.

References

(1) Liptay, W. Electrochromism and Solvatochromism. *Angew. Chemie Int. Ed.* **1969**, *8*, 177–188.

(2) Tomasi, J.; Mennucci, B.; Cammi, R. Quantum Mechanical Continuum Solvation Models. *Chem. Rev.* **2005**, *105*, 2999–3094.

(3) Mennucci, B.; Tomasi, J.; Cammi, R.; Cheeseman, J. R.; Frisch, M. J.; Devlin, F. J.; Gabriel, S.; Stephens, P. J. Polarizable Continuum Model (PCM) Calculations of Solvent Effects on Optical Rotations of Chiral Molecules. *The Journal of Physical Chemistry A* **2002**, *106*, 6102–6113.

(4) Klein, R. A.; Mennucci, B.; Tomasi, J. Ab Initio Calculations of 17O NMR-Chemical Shifts for Water. The Limits of PCM Theory and the Role of Hydrogen-Bond Geometry and Cooperativity. *The Journal of Physical Chemistry A* **2004**, *108*, 5851–5863.

(5) Warshel, A.; Levitt, M. Theoretical studies of enzymic reactions: Dielectric, electrostatic and steric stabilization of the carbonium ion in the reaction of lysozyme. *J. Mol. Bio.* **1976**, *103*, 227 – 249.

(6) Wesolowski, T. A.; Warshel, A. Frozen Density Functional Approach for Ab Initio Calculations of Solvated Molecules. *J. Phys. Chem.* **1993**, *97*, 8050–8053.

(7) Govind, N.; Wang, Y. A.; da Silva, A. J. R.; Carter, E. A. Accurate ab initio energetics of extended systems via explicit correlation embedded in a density functional environment. *Chem. Phys. Lett.* **1998**, *295*, 129–134.

(8) Bendavid, L. I.; Carter, E. A. *Status in Calculating Electronic Excited States in Transition Metal Oxides from First Principles*; Springer, 2014; pp 1–52.

(9) Wesolowski, T. A.; Shedge, S.; Zhou, X. Frozen-Density Embedding Strategy for Multilevel Simulations of Electronic Structure. *Chemical Reviews* **2015**, *115*, 5891–5928.

(10) Wesolowski, T. A. Embedding a Multideterminantal Wave Function in an Orbital-Free Environment. *Phys. Rev. A* **2008**, *77*, 012504.

(11) Hohenberg, P.; Kohn, W. Inhomogeneous Electron Gas. *Phys. Rev.* **1964**, *136*, B864–B871.

(12) Kohn, W.; Sham, L. J. Self-Consistent Equations Including Exchange and Correlation Effects. *Phys. Rev.* **1965**, *140*, A1133–A1138.

(13) Parr, R.; Yang, W. *Density-functional theory of atoms and molecules*; Oxford University Press Clarendon Press: New York Oxford England, 1989.

(14) Govind, N.; Wang, Y. A.; Carter, E. A. Electronic-structure calculations by first-principles density-based embedding of explicitly correlated systems. *J. Chem. Phys.* **1999**, *110*, 7677.

(15) Aquilante, F.; Wesołowski, T. a. Self-consistency in frozen-density embedding theory based calculations. *The Journal of Chemical Physics* **2011**, *135*, 084120.

(16) Daday, C.; König, C.; Valsson, O.; Neugebauer, J.; Filippi, C. State-specific embedding potentials for excitation-energy calculations. *J. Chem. Theory Comput.* **2013**, *9*, 2355–2367.

(17) Daday, C.; König, C.; Neugebauer, J.; Filippi, C. Wavefunction in density functional theory embedding for excited states: which wavefunctions, which densities? *ChemPhysChem* **2014**, *15*, 3205–17.

(18) Laktionov, A.; Chemineau-Chalaye, E.; Wesolowski, T. A. Frozen-density embedding theory with average solvent charge densities from explicit atomistic simulations. *Phys. Chem. Chem. Phys.* **2016**, *18*, 21069–21078.

(19) Dulak, M.; KaminÌĄski, J. W.; Wesolowski, T. A. Linearized orbital-free embedding

potential in self-consistent calculations. *International Journal of Quantum Chemistry* **2009**, *109*, 1886–1897.

(20) Dresselhaus, T.; Neugebauer, J.; Knecht, S.; Keller, S.; Ma, Y.; Reiher, M. Self-consistent embedding of density-matrix renormalization group wavefunctions in a density functional environment. *The Journal of Chemical Physics* **2015**, *142*, 044111.

(21) Wesolowski, T. A. Embedding Potentials for Excited States of Embedded Species. *J. Chem. Phys.* **2014**, *140*, 18A530.

(22) Zech, A.; Aquilante, F.; Wesolowski, T. A. Orthogonality of embedded wave functions for different states in frozen-density embedding theory. *J. Chem. Phys.* **2015**, *143*, 164106.

(23) Dreuw, A.; Weisman, J. L.; Head-Gordon, M. Long-range charge-transfer excited states in time-dependent density functional theory require non-local exchange. *The Journal of Chemical Physics* **2003**, *119*, 2943–2946.

(24) Dreuw, A.; Head-Gordon, M. Failure of Time-Dependent Density Functional Theory for Long-Range Charge-Transfer Excited States:âĂĽ The ZincbacteriochlorinâĹŠBacteriochlorin and BacteriochlorophyllâĹŠSpheroidene Complexes. *Journal of the American Chemical Society* **2004**, *126*, 4007–4016, PMID: 15038755.

(25) Laurent, A. D.; Jacquemin, D. TD-DFT benchmarks: A review. *International Journal of Quantum Chemistry* **2013**, *113*, 2019–2039.

(26) Wormit, M.; Rehn, D. R.; Harbach, P. H.; Wenzel, J.; Krauter, C. M.; Epifanovsky, E.; Dreuw, A. Investigating excited electronic states using the algebraic diagrammatic construction (ADC) approach of the polarisation propagator. *Molecular Physics* **2014**, *112*, 774–784.

(27) Harbach, P. H. P.; Wormit, M.; Dreuw, A. The third-order algebraic diagrammatic construction method (ADC(3)) for the polarization propagator for closed-shell molecules: Efficient implementation and benchmarking). *The Journal of Chemical Physics* **2014**, *141*.

(28) Dreuw, A.; Wormit, M. The algebraic diagrammatic construction scheme for the polarization propagator for the calculation of excited states. *WIREs Comput. Mol. Sci.* **2015**, *5*, 82–95.

(29) Prager, S.; Zech, A.; Aquilante, F.; Dreuw, A.; Wesolowski, T. A. First time combination of frozen density embedding theory with the algebraic diagrammatic construction scheme for the polarization propagator of second order. *The Journal of Chemical Physics* **2016**, *144*, 204103.

(30) Schirmer, J. Beyond the random-phase approximation: A new approximation scheme for the polarization propagator. *Phys. Rev. A* **1982**, *26*, 2395–2416.

(31) Trofimov, A. B.; Schirmer, J. An efficient polarization propagator approach to valence electron excitation spectra. *Journal of Physics B: Atomic, Molecular and Optical Physics* **1995**, *28*, 2299.

(32) Mertins, F.; Schirmer, J. Algebraic propagator approaches and intermediate-state representations. I. The biorthogonal and unitary coupled-cluster methods. *Phys. Rev. A* **1996**, *53*, 2140–2152.

(33) Schirmer, J.; Trofimov, A. B. Intermediate state representation approach to physical properties of electronically excited molecules. *J. Chem. Phys.* **2004**, *120*, 11449–11464.

(34) Trofimov, A. B.; Stelter, G.; Schirmer, J. A consistent third-order propagator method for electronic excitation. *The Journal of Chemical Physics* **1999**, *111*, 9982–9999.

(35) Aquilante, F.; Wesołowski, T. a. Self-consistency in frozen-density embedding theory based calculations. *The Journal of Chemical Physics* **2011**, *135*, 084120.

(36) Shao, Y.; Gan, Z.; Epifanovsky, E.; Gilbert, A. T.; Wormit, M.; Kussmann, J.; Lange, A. W.; Behn, A.; Deng, J.; Feng, X.; Ghosh, D.; Goldey, M.; Horn, P. R.; Jacobson, L. D.; Kaliman, I.; Khaliullin, R. Z.; KuÅŻ, T.; Landau, A.; Liu, J.; Proynov, E. I.; Rhee, Y. M.; Richard, R. M.; Rohrdanz, M. A.; Steele, R. P.; Sundstrom, E. J.; III, H. L. W.; Zimmerman, P. M.; Zuev, D.; Albrecht, B.; Alguire, E.; Austin, B.; Beran, G. J. O.; Bernard, Y. A.; Berquist, E.; Brandhorst, K.; Bravaya, K. B.; Brown, S. T.; Casanova, D.; Chang, C.-M.; Chen, Y.; Chien, S. H.; Closser, K. D.; Crittenden, D. L.; Diedenhofen, M.; Jr., R. A. D.; Do, H.; Dutoi, A. D.; Edgar, R. G.; Fatehi, S.; Fusti-Molnar, L.; Ghysels, A.; Golubeva-Zadorozhnaya, A.; Gomes, J.; Hanson-Heine, M. W.; Harbach, P. H.; Hauser, A. W.; Hohenstein, E. G.; Holden, Z. C.; Jagau, T.-C.; Ji, H.; Kaduk, B.; Khistyaev, K.; Kim, J.; Kim, J.; King, R. A.; Klunzinger, P.; Kosenkov, D.; Kowalczyk, T.; Krauter, C. M.; Lao, K. U.; Laurent, A. D.; Lawler, K. V.; Levchenko, S. V.; Lin, C. Y.; Liu, F.; Livshits, E.; Lochan, R. C.; Luenser, A.; Manohar, P.; Manzer, S. F.; Mao, S.-P.; Mardirossian, N.; Marenich, A. V.; Maurer, S. A.; Mayhall, N. J.; Neuscamman, E.; Oana, C. M.; Olivares-Amaya, R.; OâĂŹNeill, D. P.; Parkhill, J. A.; Perrine, T. M.; Peverati, R.; Prociuk, A.; Rehn, D. R.; Rosta, E.; Russ, N. J.; Sharada, S. M.; Sharma, S.; Small, D. W.; Sodt, A.; Stein, T.; StÃijck, D.; Su, Y.-C.; Thom, A. J.; Tsuchimochi, T.; Vanovschi, V.; Vogt, L.; Vydrov, O.; Wang, T.; Watson, M. A.; Wenzel, J.; White, A.; Williams, C. F.; Yang, J.; Yeganeh, S.; Yost, S. R.; You, Z.-Q.; Zhang, I. Y.; Zhang, X.; Zhao, Y.; Brooks, B. R.; Chan, G. K.; Chipman, D. M.; Cramer, C. J.; III, W. A. G.; Gordon, M. S.; Hehre, W. J.; Klamt, A.; III, H. F. S.; Schmidt, M. W.; Sherrill, C. D.; Truhlar, D. G.; Warshel, A.; Xu, X.; Aspuru-Guzik, A.; Baer, R.; Bell, A. T.; Besley, N. A.; Chai, J.-D.; Dreuw, A.; Dunietz, B. D.; Furlani, T. R.; Gwaltney, S. R.; Hsu, C.-P.; Jung, Y.; Kong, J.; Lambrecht, D. S.; Liang, W.; Ochsenfeld, C.; Rassolov, V. A.;

Slipchenko, L. V.; Subotnik, J. E.; Voorhis, T. V.; Herbert, J. M.; Krylov, A. I.; Gill, P. M.; Head-Gordon, M. Advances in molecular quantum chemistry contained in the Q-Chem 4 program package. *Molecular Physics* **2015**, *113*, 184–215.

(37) Cramer, C. *Essentials of computational chemistry : theories and models*; Wiley: Chichester, West Sussex, England Hoboken, NJ, 2004.

(38) Jensen, F. *Introduction to computational chemistry*; John Wiley & Sons: Chichester, England Hoboken, NJ, 2007.

(39) Szabo, A. *Modern quantum chemistry : introduction to advanced electronic structure theory*; Dover Publications: Mineola, N.Y, 1996.

(40) Gill, P. M.; Johnson, B. G.; Pople, J. A. A standard grid for density functional calculations. *Chemical Physics Letters* **1993**, *209*, 506 – 512.

(41) Wenzel, J.; Wormit, M.; Dreuw, A. Calculating core-level excitations and x-ray absorption spectra of medium-sized closed-shell molecules with the algebraic-diagrammatic construction scheme for the polarization propagator. *Journal of Computational Chemistry* **2014**, *35*, 1900–1915.

(42) Wenzel, J.; Wormit, M.; Dreuw, A. Calculating X-ray Absorption Spectra of Open-Shell Molecules with the Unrestricted Algebraic-Diagrammatic Construction Scheme for the Polarization Propagator. *Journal of Chemical Theory and Computation* **2014**, *10*, 4583–4598, PMID: 26588152.

(43) Wenzel, J.; Holzer, A.; Wormit, M.; Dreuw, A. Analysis and comparison of CVS-ADC approaches up to third order for the calculation of core-excited states. *The Journal of Chemical Physics* **2015**, *142*, 214104.

(44) Wenzel, J.; Dreuw, A. Physical Properties, Exciton Analysis, and Visualization of Core-

Excited States: An Intermediate State Representation Approach. *Journal of Chemical Theory and Computation* **2016**, *12*, 1314–1330.

(45) Plasser, F.; Wormit, M.; Dreuw, A. New tools for the systematic analysis and visualization of electronic excitations. I. Formalism. *The Journal of Chemical Physics* **2014**, *141*.

(46) Plasser, F.; Baeppler, S. A.; Wormit, M.; Dreuw, A. New tools for the systematic analysis and visualization of electronic excitations. II. Applications. *The Journal of Chemical Physics* **2014**, *141*.

(47) Plasser, F.; Thomitzni, B.; BÃďppler, S. A.; Wenzel, J.; Rehn, D. R.; Wormit, M.; Dreuw, A. Statistical analysis of electronic excitation processes: Spatial location, compactness, charge transfer, and electron-hole correlation. *Journal of Computational Chemistry* **2015**, *36*, 1609–1620.

(48) Krauter, C. M.; Schimmelpfennig, B.; Pernpointner, M.; Dreuw, A. Algebraic diagrammatic construction for the polarization propagator with spin-orbit coupling. *Chemical Physics* **2017**, *482*, 286 – 293, Electrons and nuclei in motion - correlation and dynamics in molecules (on the occasion of the 70th birthday of Lorenz S. Cederbaum).

(49) Hanwell, M.; Curtis, D.; Lonie, D.; Vandermeersch, T.; Zurek, E.; Hutchison, G. Avogadro: an advanced semantic chemical editor, visualization, and analysis platform. *Journal of Cheminformatics* **2012**, *4*, 17.

(50) Persistence of Vision Raytracer Pty. Ltd, POV-Ray 3.7.

(51) Willighagen, E.; Howard, M. Fast and Scriptable Molecular Graphics in Web Browsers without Java3D. *Nature Precedings* **2007**,

(52) Dennington, R.; Keith, T.; Millam, J. GaussView Version 5. Semichem Inc., Shawnee Mission, KS, 2009.

(53) Becke, A. D. Density functional calculations of molecular bond energies. *The Journal of Chemical Physics* **1986**, *84*, 4524–4529.

(54) Lee, C.; Yang, W.; Parr, R. G. Development of the Colle-Salvetti correlation-energy formula into a functional of the electron density. *Physical Review B* **1988**, *37*, 785–789.

(55) Perdew, J. P.; Burke, K.; Ernzerhof, M. Generalized Gradient Approximation Made Simple. *Physical Review Letters* **1996**, *77*, 3865–3868.

(56) Perdew, J. P. Density-functional approximation for the correlation energy of the inhomogeneous electron gas. *Physical Review B* **1986**, *33*, 8822–8824.

(57) Perdew, J. P.; Chevary, J. A.; Vosko, S. H.; Jackson, K. A.; Pederson, M. R.; Singh, D. J.; Fiolhais, C. Atoms, molecules, solids, and surfaces: Applications of the generalized gradient approximation for exchange and correlation. *Physical Review B* **1992**, *46*, 6671–6687.

(58) Becke, A. D. Density–functional thermochemistry. III. The role of exact exchange. *The Journal of Chemical Physics* **1993**, *98*, 5648–5652.

(59) Shao, Y.; Head-Gordon, M.; Krylov, A. I. The spin–flip approach within time-dependent density functional theory: Theory and applications to diradicals. *The Journal of Chemical Physics* **2003**, *118*, 4807–4818.

(60) Adamo, C.; Barone, V. Toward reliable density functional methods without adjustable parameters: The PBE0 model. *The Journal of Chemical Physics* **1999**, *110*, 6158–6170.

(61) Peverati, R.; Truhlar, D. G. Communication: A global hybrid generalized gradient approximation to the exchange-correlation functional that satisfies the second-order density-gradient constraint and has broad applicability in chemistry. *The Journal of Chemical Physics* **2011**, *135*, 191102.

(62) Gill, P. M. W. A new gradient-corrected exchange functional. *Molecular Physics* **2010**, *89*, 433–445.

(63) Yu, H. S.; Zhang, W.; Verma, P.; He, X.; Truhlar, D. G. Nonseparable exchange–correlation functional for molecules, including homogeneous catalysis involving transition metals. *Phys. Chem. Chem. Phys.* **2015**, *17*, 12146–12160.

(64) Dunning, T. H. Gaussian basis sets for use in correlated molecular calculations. I. The atoms boron through neon and hydrogen. *The Journal of Chemical Physics* **1989**, *90*, 1007–1023.

(65) Lundqvist, S., March, N. H., Eds. *Theory of the inhomogeneous electron gas*; Physics of solids and liquids; Plenum press: New York and N.Y and London, 1983.

(66) Ditchfield, R.; Hehre, W. J.; Pople, J. A. Self–Consistent Molecular–Orbital Methods. IX. An Extended Gaussian–Type Basis for Molecular–Orbital Studies of Organic Molecules. *The Journal of Chemical Physics* **1971**, *54*, 724–728.

(67) Hehre, W. J.; Ditchfield, R.; Pople, J. A. Self—Consistent Molecular Orbital Methods. XII. Further Extensions of Gaussian—Type Basis Sets for Use in Molecular Orbital Studies of Organic Molecules. *The Journal of Chemical Physics* **1972**, *56*, 2257–2261.

(68) Hariharan, P. C.; Pople, J. A. The influence of polarization functions on molecular orbital hydrogenation energies. *Theoretica Chimica Acta* **1973**, *28*, 213–222.

(69) Luzanov, A. V.; Sukhorukov, A. A.; Umanskii, V. . Application of transition density matrix for analysis of excited states. *Theoretical and Experimental Chemistry* **1976**, *10*, 354–361.

(70) Martin, R. L. Natural transition orbitals. *The Journal of Chemical Physics* **2003**, *118*, 4775–4777.

(71) Mayer, I. Using singular value decomposition for a compact presentation and improved interpretation of the CIS wave functions. *Chemical Physics Letters* **2007**, *437*, 284–286.

(72) Prager, S.; Burghardt, I.; Dreuw, A. Ultrafast C Spiro –O Dissociation via a Conical Intersection Drives Spiropyran to Merocyanine Photoswitching. *The Journal of Physical Chemistry A* **2014**, *118*, 1339–1349.

(73) Lin, Y.-S.; Li, G.-D.; Mao, S.-P.; Chai, J.-D. Long-Range Corrected Hybrid Density Functionals with Improved Dispersion Corrections. *Journal of Chemical Theory and Computation* **2013**, *9*, 263–272.

(74) Krysanov, S.; Alfimov, M. Ultrafast formation of transients in spiropyran photochromism. *Chemical Physics Letters* **1982**, *91*, 77–80.

(75) Ernsting, N. P. Transient optical absorption spectroscopy of the photochemical spiropyran-merocyanine conversion. *Chemical Physics Letters* **1989**, *159*, 526–531.

(76) Ernsting, N. P.; Dick, B.; Arthen-Engeland, T. The primary photochemical reaction step of unsubstituted indolino-spiropyrans. *Pure and Applied Chemistry* **1990**, *62*.

(77) Kohl-Landgraf, J.; Braun, M.; Özçoban, C.; Gonçalves, D. P. N.; Heckel, A.; Wachtveitl, J. Ultrafast Dynamics of a Spiropyran in Water. *Journal of the American Chemical Society* **2012**, *134*, 14070–14077.

(78) Kohl-Landgraf, J.; Braun, M.; Özçoban, C.; Goncalves, D.; Heckel, A.; Wachtveitl, J.; Chergui, M.; Taylor, A.; Cundiff, S.; Vivie-Riedle, R. d.; Yamagouchi, K. Dynamics of a photochromic spiropyran under aqueous conditions. *EPJ Web of Conferences* **2013**, *41*, 05009.